

Bearing capacity assessment of reinforced concrete slab –special-shaped column connections

Wei Zhang¹, Jianyang Xue^{*1}, Jinjun Xu², Baoxin Li¹ and Jinghui Wei¹

¹ School of Civil Engineering, Xi'an University of Architecture & Technology, Xi'an 710055, China

² College of Civil Engineering, Nanjing Tech University, Nanjing, 211816, China

(Received July 19, 2021, Revised November 10, 2022, Accepted December 14, 2022)

Abstract. Most failure modes in flat slabs are punch failure. However, in practice, there are many instances where punching failure is preceded by bending failure, or the actual failure mode is bending-punching failure. In order to obtain the reasonable result of bending failure, an accurate method is proposed to estimate the flexural capacity of slab–special-shaped column (cruciform, L-shaped, T-shaped) connections based on the yield-line theory, and the theoretical model is verified by comparing with the collected experimental results. In addition, the influence of column section shape and column limb length to thickness ratio (c_2/c_1) on the bearing capacity was discussed. The results show that the column section shape has an effect on the bending capacity of slab–column connection, but the effect was not significant. At the same time, the column limb length to thickness ratio (c_2/c_1) has little effect on the bending capacity, which can be ignored.

Keywords: bending failure; failure load; slab-column connections; special-shaped column; yield-line theory

1. Introduction

The slab–column structures are simple in form and high availability in space, and have been widely used in various construction industries (Shubha *et al.* 2014, Bhowmik *et al.* 2017 and Tovi *et al.* 2017). For the slab–column structures, the ability of resisting internal force and deformation of connections are relatively weak, easy to occur punching shear failure, what is more, cause the collapse of the whole structure. Therefore, the research on the mechanical behavior of slab–column connection has not stopped. Ma and Lü (2001) completed the tests of six slab–column connections under vertical and horizontal repeated loads, and deduced the calculating formulae of the punching shear and bending strengths of slab–column connections. Sagaseta *et al.* (2014) investigated the effect of loading conditions (unidirectional or bidirectional bending) on the punching shear strength of concrete slabs. The results showed that the column section shape will lead to the concentration of shear stresses at the control perimeter. Alam *et al.* (2016) designed and completed 15 punching tests of slab–column connections to explore the influence of boundary constraint, bending reinforcement and slab thickness on the connections performance and punching capacity. The test results showed that the influence of bending reinforcement on the connection bearing capacity was smaller than that of boundary constraint and slab thickness. In addition, a lot of work has been done to improve the punching shear capacity of slab–column

connections. Mamede *et al.* (2013) studied the contribution of rational use of high strength concrete (HSC) to the punching shear capacity of slab–column connections. The results show that use of the HSC showed excellent results in terms of punching strength. Meanwhile, the compressive strength of concrete can improve the punching capacity more than the tensile strength of concrete (Inácio *et al.* 2020). Zhou *et al.* (2021) proposed a new type of slab–column connection embedded in a steel skeleton, and studied the punching shear performance of composite connection. The test results show that the embedded steel skeleton can effectively improve the punching capacity of slab–column connection and improve the ductility of the structure.

At present, in the study of the ultimate bearing capacity of slab–column connection, the punching shear capacity is usually calculated by the regression formula of punching shear test, and then the bending capacity obtained from the yield-line theory is used to check the punching shear capacity, and the smaller value of the two is taken as the bearing capacity of the slab–column connection. When calculating the bending capacity of slab–column connections, GB 50010-2010, ACI Committee 318, and Eurocode 2 have similar calculation methods, which all estimate the bending capacity of slab–column connections based on the yield-line theory. The yield-line theory was first applied to study on the bending capacity of the slab–square column connection (Park and Gambe 1980). On this basis, Baskaran and Morley (2004) referring to different codes, gave a formula for calculating the bending capacity of slab–square column connection considering the support conditions. However, it can be found that these studies mostly take square columns as the research objects, and only rectangular columns and circular columns are

*Corresponding author, Ph.D., Professor,
E-mail: jianyang_xue@163.com

considered to influence the shape of column section (Cho *et al.* 2006 and Liu 2006). However, the test studies and theoretical analyses of slab–special-shaped column connections have not reported in public literature.

In addition, with the in-depth study on the failure mechanism of slab–column connections, Chanthabouala and Teng (2015) and Goswami *et al.* (2019) found that the slab–column connection has punching failure characteristics when the reinforcement ratio (ρ) is large. When the reinforcement ratio in the slab is low, the punching failure usually shows obvious bending deformation before it occurs. Bending failure is marked by the formation of yield hinge line at the slab surface, and punching failure is marked by the formation of punching failure cone in the slab and the punching off from the tensile surface of the slab (Ghali *et al.* 2015). However, the actual reinforcement of the slab belongs to the normal reinforcement ratio, which is neither very high nor very low. The mode of failure will not be clear because it can be a combination of bending failure and punching failure. The research results of Thomas (2004) and Stein *et al.* (2007) also showed a strong correlation between the punching and bending characteristics of the slab–column connection. In this case, how to accurately identify the failure mode and assess its ultimate bearing capacity is particularly important. Therefore, this paper studied the bending capacity of slab–special-shaped column connections (cruciform column, T-shaped column and L-shaped column) by using yield-line theory. This is new research on special-shaped column. This will help to open the application prospect of special-shaped column structure and provide help for the structural design of slab–special-shaped column.

2. Tests dataset

Through a large number of literature selection, the results of bending of 32 slab–column connections in literature (Liu and Huang 2004, Cai *et al.* 2006, Guandalini *et al.* 2009, Guidotti 2010, Yi *et al.* 2016, Teng *et al.* 2018 and Pinto *et al.* 2018) are collected. See Appendix A1 for the test data.

Since the tests in the literature are completed in different countries and laboratories, there may be differences in test design, material performance index, geometric shape,

loading mode, etc. To achieve the unification of key test data, the data are described as follows:

- (1) The selected test data are all the test results of slab–column connections under bending failure;
- (2) The selected test data are all use the international system of units (kN);
- (3) The shape of the reinforced concrete slab is square, the vertical load is applied along the column head by the actuator, and the boundary conditions are simply supported on four sides.

3. Bending capacity based on yield-line theory

The yield-line theory is an upper bound method for RC slabs, in which the ultimate load of slab is estimated by assuming a failure mechanism compatible with boundary conditions (Quintas 2003, Elsheikh 2006 and Braestrup 2008). For a given slab, the ultimate load obtained by yield-line theory may be correct or larger, because this method is an upper bound method. Therefore, various possible failure mechanisms of the slab should be considered to ensure that the bearing capacity of the slab is not overestimated. It should be noted that the yield-line theory assumes a bending failure mode, that is, the slab is assumed to have sufficient shear strength to prevent shear failure.

3.1 The condition of slab under ultimate load

3.1.1 Reinforcement in slab

When the yield-line theory is used to solve the ultimate load of slabs, the ultimate resistance moment per unit width is usually assumed to be a fixed value for the convenience of calculation. In this case, the reinforcement in the two directions of the slab is generally arranged at right angles, and the reinforcement is uniform and isotropic. It is worth noting that the reinforcement in the two directions of the slab can be different, and the reinforcement at the top and bottom of the slab can also be different. It only needs to meet the requirement that the reinforcement area per unit width is equal. It should be pointed out that the study of yield-line model in this paper is also based on this assumption.

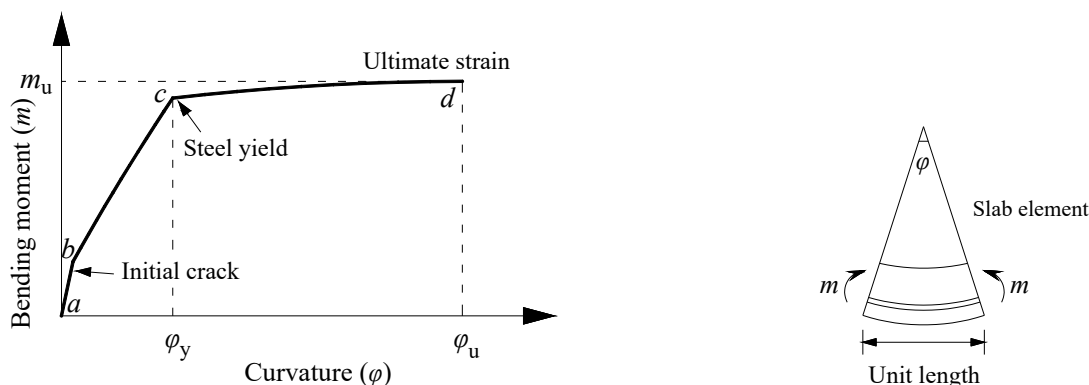


Fig. 1 Bending moment-curvature relationship of reinforced concrete slab section

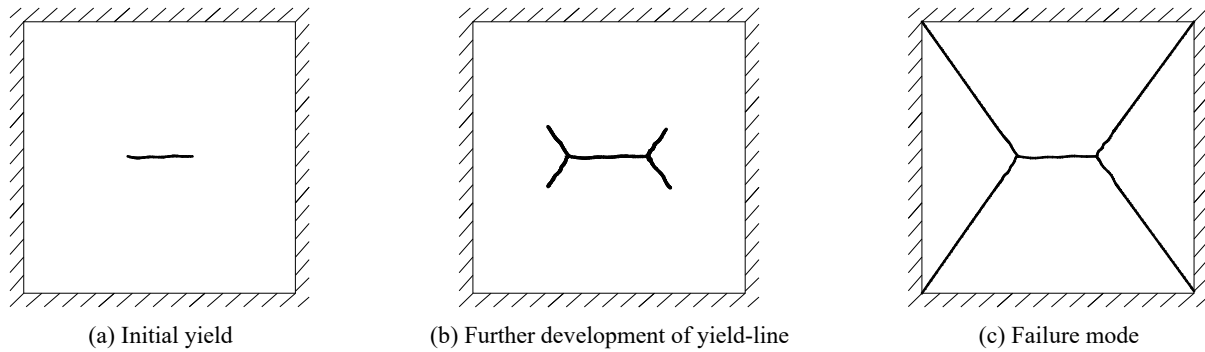


Fig. 2 Forming process of yield-line of simply supported slab

3.1.2 Performance of the slab section

Since the yield-line theory assumes a bending failure mode, which means that the slab section should have enough ductility to produce plastic rotation on the dangerous section and form plastic hinge on the whole slab. The effective ductility depends on the shape of the bending moment-curvature curve of the section. Fig. 1 shows the bending moment-curvature relationship of reinforced concrete slab section. The relationship curve can be roughly divided into three stages: the initial elastic stage before concrete cracking (*a-b* in Fig. 1); The straight line stage (*b-c* in Fig. 1) before yielding of tensile reinforcement; Finally, the last is an almost horizontal straight line (*c-d* in Fig. 1), where the resistance bending moment of the section keeps close to the limit value until the concrete reaches its ultimate strain. The section ductility is measured by the curvature ductility coefficient, which is defined as the ratio of the curvature when the concrete reaches the ultimate strain to the curvature when the tensile reinforcement begins to yield, φ_u / φ_y . Obviously, for most slabs, in order to ensure that the failure mode is bending failure, it requires that the slab section has enough ductility. Accordingly, the ratio of tensile reinforcement should be low enough.

3.1.3 Yield-line model and basic assumptions

During the loading process, the deformation of reinforced concrete (RC) slab goes through three stages: in the first stage, the initial bending moment appears when the load is small; In the second stage, with the increase of load, the tensile reinforcement begins to yield, the curvature of yield section changes greatly, and the bending moment redistributes; In the third stage, the load increases again, the severe crack line (yield-line) subdivides the slab into failure mechanism, and the yield-line system of failure mechanism is the yield-line mode (Kennedy and Goodchild 2004). The forming process of yield-line mode of simply supported slab is shown in Fig. 2, and the oblique lines in Fig. 2 represent simply supported edges. It should be pointed out that the yield-line is actually an idealization of a severely cracked zone through which the tensile reinforcement has yielded.

The basic assumptions of the yield-line model are as follows (Burgess 2017):

- (1) The yield-line is generated at the maximum bending moment when the slab is close to failure

and divides the slab into several blocks connected by the yield-line, making the slab becomes a variable system.

- (2) The yield-line is the crack line generated by the yielding of the reinforcement. The ultimate moment of resistance on the yield-line remains unchanged, but the angle of rotation can continue to increase.
- (3) The elastic deformation of each slab is negligible compared with the large displacements generated by each slab along the yield-line, and each slab can be regarded as a rigid body.
- (4) Among all possible failure mechanisms, only the one that produces the smallest failure load is the most important and the most dangerous.

3.2 Analysis method of virtual work principle

The principle of virtual work can be stated as follows: assuming that the rigid body is in equilibrium under the action of a system of forces, the sum of the work done by these forces will be zero if the rigid body produces any small translocation (Liu and Zhang 2008). Therefore, the displacement $\delta(x, y)$ produced at all points in the slab and the angle of rotation of each slab to the yield-line can be obtained by selecting a suitable point in the slab and making that point produce a small displacement (δ) under external load. Assuming that the unit concentrated load P_i acts vertically on the slab, the virtual work done by the external force is as follows

$$W_e = \sum P_i \delta(x, y) \quad (1)$$

Since there is a relative angle of rotation between the two sides of the yield-line, but there is no relative displacement, the work done on the yield-line is generated only by the ultimate bending moment, while the sum of work done by the torque and shear force is zero. The virtual work done by the unit length ultimate bending moment (m_u) on the yield-line of length (l_0) is as follows

$$W_i = - \sum m_u \theta_n l_0 \quad (2)$$

where θ_n is the relative angle of rotation between the two sides of the yield-line. Thus, the virtual work equation can

be written as follows

$$\sum P_i \delta(x, y) - \sum m_u \theta_n l_0 = 0 \quad (3)$$

3.3 Ultimate resistance moment at yield-line

The yield-line theory is applicable to slabs with uniform reinforcement. Usually, the reinforcement in the slab are arranged at right angles in both directions, the cross-sectional area of the steel bars per unit width is the same, and the ultimate bending moment per unit width is a fixed value. However, in some cases, the angle of the reinforcement in the slab is not 90° in both directions, and there is a torque in addition to the ultimate bending moment along the yield-line, which needs further exploration. For the convenience of discussion, only the bending failure of the slab with a reinforcement angle of 90° is studied in this paper.

Assuming that m_u is the ultimate bending moment on the yield-line, when the yield-line is at right angles to the reinforcement, the bending moment per unit width generated by the reinforcement can be expressed as (Zhu *et al.* 1993)

$$m_u = A_s f_y h_0 \left(1 - 0.5 \rho \frac{f_y}{f_{cm}} \right) \quad (4)$$

where A_s is the area of tensile reinforcement per unit width; f_y is design value of tensile reinforcement strength; h_0 is effective thickness of the slab; f_{cm} is design value of compressive strength of concrete; ρ is reinforcement rate of tensile reinforcement in the slab.

3.4 Calculation of bending capacity for slab-column connections

Scholars have done a lot of research on the ultimate load of traditional slab–square column connections under concentrated load (Ma *et al.* 2021), but there is little research on the bending ultimate load of slab–special-shaped column connections under concentrated load. According to the yield-line theory, the bending capacity calculation equation of slab–special-shaped column connections under concentrated load is established in this paper.

Osman *et al.* (2000) studied the theoretical solution of the yield-line for the bending capacity of the slab–square column connection with four simply supported edges and orthogonal isotropy. The form of the yield-line is shown in Fig. 3 (the thick line in the Fig. 3 represents the yield-line), and the calculation formula of the bending capacity is shown in Eq. (5). The results show that the position of the yield-line is symmetrically distributed and the angle between the yield-line and the x -axis is 22.5°(α).

$$P_{flex} = 8m_u \frac{L-c}{L_0-c} \left[\frac{L}{L-c} + 2(\sqrt{2}-1) \right] \quad (5)$$

where L is the side length of the slab; L_0 is the effective side length of slab; c is the side length of square column.

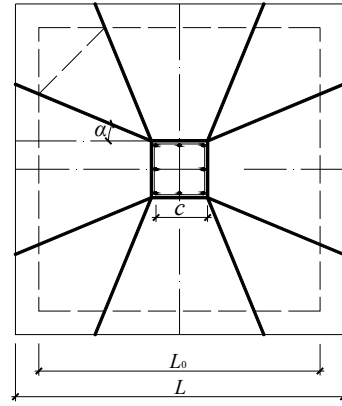


Fig. 3 Yield-line model of slab–square column connection

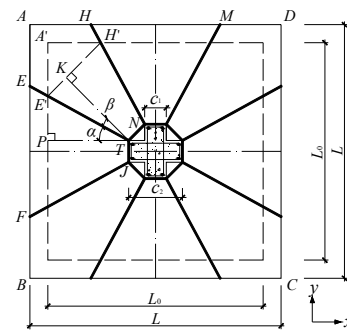


Fig. 4 Yield-line model of slab–cruciform column connection

3.4.1 Theoretical solution of yield-line for bending capacity of slab–cruciform column

According to the failure mode of yield-line of slab–square column connection under concentrated load, it is assumed that the yield-line of slab–cruciform connection under concentrated load is shown in Fig. 4. According to the yield-line theory, the bending capacity is deduced by virtual work equation.

In Fig. 4, c_1 is column section limb thickness; c_2 is column section limb length.

It can be found from Fig. 4 that the work done by the ultimate bending moment is caused by the bending moments on eight isosceles trapezoidal blocks. When the column occurs a unit of virtual displacement relative to the slab support, the external work (W_e) done by the column load P is

$$W_e = P \times 1 = P \quad (6)$$

The virtual work (W_i) done by the internal force in the slab is the internal work (considering symmetry), which is obtained according to Eq. (2)

$$W_i = 4W_i(ETJF) + 4W_i(AHNT E) \quad (7)$$

where the internal virtual work of the slab $ETJF$ and $AHNT E$ is as follows

$$W_i(ETJF) = m_u \times EF/TP \quad (8)$$

$$W_i(AHNT E) = m_x \times \frac{AE \cos(\alpha + \beta)}{TK} + m_y \times AH \cos(\alpha + \beta) / TK \quad (9)$$

According to the geometric relationship, Eqs. (8) and (9) can be changed into Eqs. (10) and (11)

$$W_i(ETJF) = \frac{2m_u}{L_0 - c_2} [c_1 + (L - c_2) \tan \alpha] \quad (10)$$

$$W_i(AHNT E) = m_u [(L - c_1) - (L - c_2) \tan \alpha] \cos\left(\frac{\pi}{4}\right) / TK \quad (11)$$

where TK can be found by the geometric relationship as followed

$$TK = \frac{\sqrt{2}(L_0 - c_2)}{4} (1 + \tan \alpha) \quad (12)$$

According to Eqs. (7)-(12), from the imaginary work Eq. (3), the flexural capacity (P_{flex}) is assessed as follows

$$P_{\text{flex}} = \frac{8m_u}{L_0 - c_2} \left[c_1 + (L - c_2) \tan \alpha + \frac{(L - c_1) - (L - c_2) \tan \alpha}{1 + \tan \alpha} \right] \quad (13)$$

$$W_i(FTJSB) = m_u \left[\left(\frac{(L + c_2)}{2} - c_1 \right) - \frac{(L - c_2) \tan \eta}{2} \right] \cos \times \frac{\left(\frac{\pi}{2} - \varphi\right)}{JI} + m_u \left[\frac{(L - c_1)}{2} - \frac{(L - c_2) \tan \theta}{2} \right] \cos \varphi / JI \quad (23)$$

where $\alpha = \tan^{-1} \left(\sqrt{1 + \frac{L - c_1}{L - c_2}} - 1 \right)$.

3.4.2 Theoretical solution of yield-line for bending capacity of slab–T-shaped column connection

Suppose that the yield-line of slab–T-shaped column connection under bending limit state is shown in Fig. 5, and the bending capacity derived from virtual work equation is as follows.

In Fig. 5, λ, θ is the direction angle of yield-line.

Obviously, the yield-line model consists of triangles, parallelograms and trapezoids. The external force work done by the column load can be calculated according to Eq. (1)

$$W_e = P \times 1 = P \quad (14)$$

The internal virtual work is calculated according to Eq. (2)

$$W_i = 2W_i(ENTF) + 2W_i(AHNE) + 2W_i(FTJSB) + W_i(HMON) + W_i(SVWJ) \quad (15)$$

$$W_i(ENTF) = m_x \times EF / NP \quad (16)$$

$$W_i(AHNE) = m_x \times \frac{AE \cos(\alpha + \beta)}{NK} + m_y \times AH \cos(\alpha + \beta) / NK \quad (17)$$

$$W_i(FTJSB) = m_x \times \frac{FB \cos\left(\frac{\pi}{2} - \varphi\right)}{JI} + m_y \times BS \cos \varphi / JI \quad (18)$$

$$W_i(HMON) = m_y \times HM / NR \quad (19)$$

$$W_i(SVWJ) = m_y \times SV / JG \quad (20)$$

According to the geometric relationship, the following simplified results can be obtained

$$\alpha + \beta = \frac{\pi}{4}, \quad \eta = \theta, \quad \lambda + \theta = \varphi, \\ \tan \varphi = 2, \quad \tan(\pi/2 - \varphi) = 1/2$$

where the internal virtual work of the slab $ENTF$, $AHNE$, $FTJSB$, $HMON$ and $SVWJ$ is as follows

$$W_i(ENTF) = \frac{m_u \left[c_1 + \frac{(L - c_2)}{2} (\tan \alpha + \tan \eta) \right]}{\frac{(L_0 - c_2)}{2}} \quad (21)$$

$$W_i(AHNE) = m_u [(L - c_2) - (L - c_2) \tan \alpha] \times \cos \frac{\pi}{4} / NK \quad (22)$$

$$W_i(HMON) = 2m_u [c_2 + (L - c_2) \tan \alpha] / (L_0 - c_2) \quad (24)$$

$$W_i(SVWJ) = 2m_u [c_1 + (L - c_2) \tan \theta] / (L_0 - c_2) \quad (25)$$

The results of TW , JI and NK can be obtained by using the geometric relationship

$$NK = \frac{\sqrt{2}(L_0 - c_2)}{4} (1 + \tan \alpha) \quad (26)$$

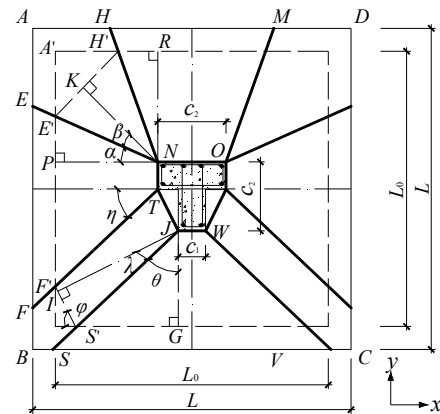


Fig. 5 Yield-line model of slab–T-shaped column connection

$$JI = \frac{(L_0 - c_2)}{2\sqrt{5}}(1 + \tan \theta) \quad (27)$$

According to Eqs. (15)-(27), from the imaginary work Eq. (3), the flexural capacity (P_{flex}) is assessed as follows

$$\begin{aligned} P_{\text{flex}} = & \frac{4m_u}{L_0 - c_2} \left[c_1 + \frac{(L - c_2)}{2} (\tan \alpha + \tan \eta) \right] + \frac{4m_u(L - c_2)}{(L_0 - c_2)} \times \frac{(1 - \tan \alpha)}{(1 + \tan \alpha)} \\ & + \frac{8m_u}{(L_0 - c_2)(1 + \tan \theta)} \times \left[\left(\frac{(L + c_2)}{2} - c_1 \right) - \frac{(L - c_2)}{2} \tan \theta \right] \\ & + \frac{2m_u}{(L_0 - c_2)} \times [c_1 + c_2 + (L - c_2)(\tan \alpha + \tan \theta)] + \frac{4m_u}{(L_0 - c_2)(1 + \tan \theta)} \left[\frac{(L - c_1)}{2} - \frac{(L - c_2)}{2} \tan \theta \right] \end{aligned} \quad (28)$$

The partial derivatives of α , θ are taken separately, the partial derivatives are zero, and the minimum upper limit solution of the bending capacity can be found.

$$\begin{aligned} \frac{dP}{d\alpha} = 0, \quad \alpha &= \arctan(\sqrt{2} - 1) \\ \frac{dP}{d\theta} = 0, \quad \theta &= \arctan\left(\sqrt{\frac{5(3L - 2c_1 - c_2)}{3(L - c_2)}} - 2\right) \end{aligned}$$

The flexural capacity (P_{flex}) is assessed as follows

$$\begin{aligned} P_{\text{flex}} = & 8m_u \frac{(L - c_2)(\sqrt{2} - 1)}{(L_0 - c_2)} + \frac{2m_u(3c_1 + c_2)}{(L_0 - c_2)} + \frac{2m_u(L - c_2)}{(L_0 - c_2)} \times (\tan \theta + \tan \eta) \\ & + \frac{8m_u}{(L_0 - c_2)(1 + \tan \theta)} \left[\left(\frac{(L + c_2)}{2} - c_1 \right) - \frac{(L - c_2)}{2} \times \tan \theta \right] \\ & + \frac{4m_u}{(L_0 - c_2)(1 + \tan \theta)} \left[\frac{(L - c_1)}{2} - \frac{(L - c_2)}{2} \tan \theta \right] \end{aligned} \quad (29)$$

where $\tan \theta = \left(\sqrt{\frac{5(3L - 2c_1 - c_2)}{3(L - c_2)}} - 2 \right)$.

3.4.3 Theoretical solution of yield-line bending capacity of slab-L-shaped column connection

In the same way, it is assumed that the yield-line model of slab-L-shaped column connection under bending limit state is shown in Fig. 6.

The yield-line model consists of triangles and isosceles trapezoids centered on L-shaped columns. Internal virtual

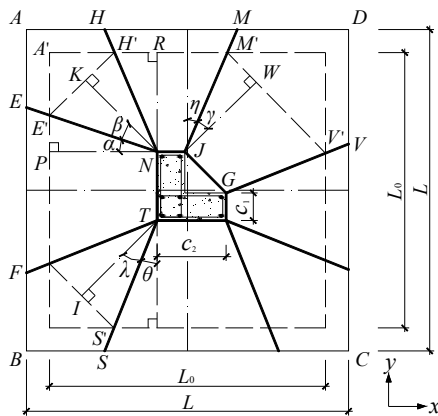


Fig. 6 Yield-line model of slab-L-shaped column connection

work can be expressed as

$$W_i = 2W_i(ENTF) + 2W_i(AHNE) + 2W_i(HMJN) + W_i(FTSB) + W_i(MDVGJ) \quad (30)$$

where the internal virtual work of the each sub-block is as follows

$$W_i(ENTF) = m_x \times EF/NP \quad (31)$$

$$\begin{aligned} W_i(AHNE) = & m_x \times \frac{AE \cos(\alpha + \beta)}{NK} \\ & + m_y \times AH \cos(\alpha + \beta) / NK \end{aligned} \quad (32)$$

$$W_i(HMJN) = m_y \times HM/NR \quad (33)$$

$$\begin{aligned} W_i(FTSB) = & m_x \times \frac{FB \cos(\lambda + \theta)}{TI} \\ & + m_y \times BS \cos(\lambda + \theta) / TI \end{aligned} \quad (34)$$

$$\begin{aligned} W_i(MDVGJ) = & m_x \times \frac{DV \cos(\gamma + \eta)}{JW} \\ & + m_y \times MD \cos(\gamma + \eta) / JW \end{aligned} \quad (35)$$

Through the geometric relationship of each sub-block, the following relationship can be obtained

$$\alpha + \beta = \frac{\pi}{4}, \quad \gamma + \eta = \frac{\pi}{4}, \quad \lambda + \theta = \pi/4$$

Combined with Eq. (30), the results are as follows

$$W_i(ENTF) = m_u \times \frac{\left[c_2 + \frac{(L - c_2)}{2} (\tan \alpha + \tan \theta) \right]}{\frac{(L_0 - c_2)}{2}} \quad (36)$$

$$W_i(AHNE) = 2m_u \times \frac{\left(\frac{L - c_2}{2} - \frac{L - c_2}{2} \tan \alpha \right) \cos \frac{\pi}{4}}{NK} \quad (37)$$

$$W_i(HMJN) = m_u \times \frac{\left[c_1 + \frac{(L - c_2)}{2} (\tan \alpha + \tan \eta) \right]}{\frac{(L_0 - c_2)}{2}} \quad (38)$$

$$W_i(FTSB) = 2m_u \times \frac{\left[\frac{L-c_2}{2} - \frac{L-c_2}{2} \tan \theta \right] \cos \frac{\pi}{4}}{TI} \quad (39)$$

$$W_i(MDVGJ) = 2m_u \times \left[\frac{L+c_2-2c_1}{2} - \frac{L-c_2}{2} \tan \eta \right] \times \frac{\cos \frac{\pi}{4}}{JW} \quad (40)$$

NK , TI , JW can be obtained by geometric relation

$$NK = \frac{\sqrt{2}(L_0 - c_2)}{4} (1 + \tan \alpha) \quad (41)$$

$$TI = \frac{\sqrt{2}(L_0 - c_2)}{4} (1 + \tan \theta) \quad (42)$$

$$JW = \frac{\sqrt{2}(L_0 - c_2)}{4} (1 + \tan \eta) \quad (43)$$

According to Eqs. (30)-(43), from virtual work equation Eq. (3), the flexural capacity (P_{flex}) is assessed as follows

$$P_{\text{flex}} = \frac{4m_u}{L_0 - c_2} \left[c_2 + \frac{(L - c_2)(\tan \alpha + \tan \theta)}{2} \right] + \frac{4m_u(L - c_2)(1 - \tan \alpha)}{(L_0 - c_2)(1 + \tan \alpha)} + \frac{4m_u}{L_0 - c_2} \left[c_1 + \frac{(L - c_2)}{2} (\tan \alpha + \tan \eta) \right] + \frac{2m_u(L - c_2)}{(L_0 - c_2)} \times \frac{(1 - \tan \theta)}{(1 + \tan \theta)} + \frac{2m_u}{(L_0 - c_2)} \times \left[\frac{L + c_2 - 2c_1 - (L - c_2) \tan \eta}{1 + \tan \eta} \right] \quad (44)$$

The minimum upper bound solution of bending capacity is obtained by calculating the partial derivative of α , η and θ and making the partial derivative equal to zero.

$$\alpha = \tan^{-1}(\sqrt{2} - 1), \quad \eta = \tan^{-1} \left(\sqrt{\frac{2L - 2c_1}{L - c_2} - 1} \right),$$

$$\theta = \tan^{-1}(\sqrt{2} - 1)$$

The flexural capacity (P_{flex}) is assessed as follows

$$P_{\text{flex}} = 2m_u \frac{L - c_2}{L_0 - c_2} \left[6(\sqrt{2} - 1) + \tan \eta \right] + \frac{4m_u(c_1 + c_2)}{(L_0 - c_2)} + \frac{2m_u}{L_0 - c_2} \times \left[\frac{L + c_2 - 2c_1 - (L - c_2) \tan \eta}{1 + \tan \eta} \right] \quad (45)$$

where $\tan \eta = \sqrt{\frac{2L - 2c_1}{L - c_2} - 1}$.

4. Discussing

4.1 Comparison between the calculated results and the test results

In order to verify the correctness of the theoretical solution of the yield-line of the bending capacity of the slab–special-shaped column connection, the calculation results of the bending capacity derived from the formula are compared with the test results by using the previously

established test database, as shown in Fig. 7. To simplify the calculation, it is assumed that the simply supported position is at the edge of the slab, $L = L_0$.

Fig. 7 shows the comparison results between the calculated results and the test results. The comparison results take the test results (P_u) of each literature as the horizontal coordinate and the bending capacity calculated results (P_{flex}) as the horizontal coordinate. The discreteness between the calculated results and the test results is very small, and there is a good consistency, in which $R^2 = 0.985$, $\text{RMSE} = 18$, which shows that the formula derived in this paper has a high accuracy for design and evaluation.

In order to further demonstrate the reliability of the formula, the ratio of the experimental value of each literature and the theoretical prediction value of bending capacity (P_u/P_{flex}) is taken as the vertical coordinate, and the

reinforcement ratio (ρ) is taken as the horizontal coordinate. The evaluation results are shown in Fig. 8.

For convenience of understanding and explanation, a black auxiliary line is drawn in Fig. 8, indicating the case where the ratio of the experimental results to the theoretical results is 1. It can be found that for the scattered points whose ratio results are higher than the auxiliary line, the corresponding test results in the literature are all bending failure, and the corresponding reinforcement ratio is usually relatively small, as shown in Figs. 8(a), 8(b), 8(c) and 8(d). However, for the scattered points with the ratio results below the auxiliary line, the test phenomenon often shows the brittleness characteristic. During the failure process, the bending strength of the specimen was not fully exerted (the reinforcement ratio was greater than 1.3%), and the punching shear failure plays a controlling role, as shown in Fig. 8(f).

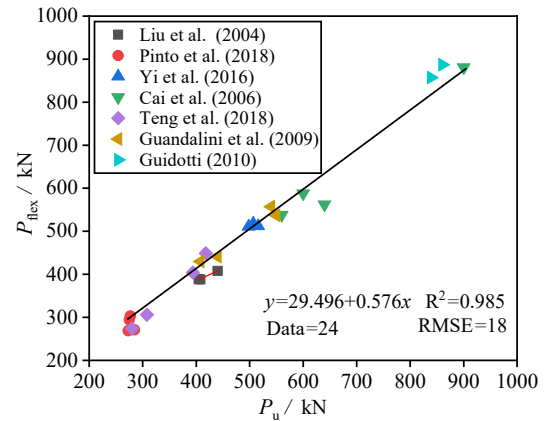


Fig. 7 Comparison of calculated results and test results

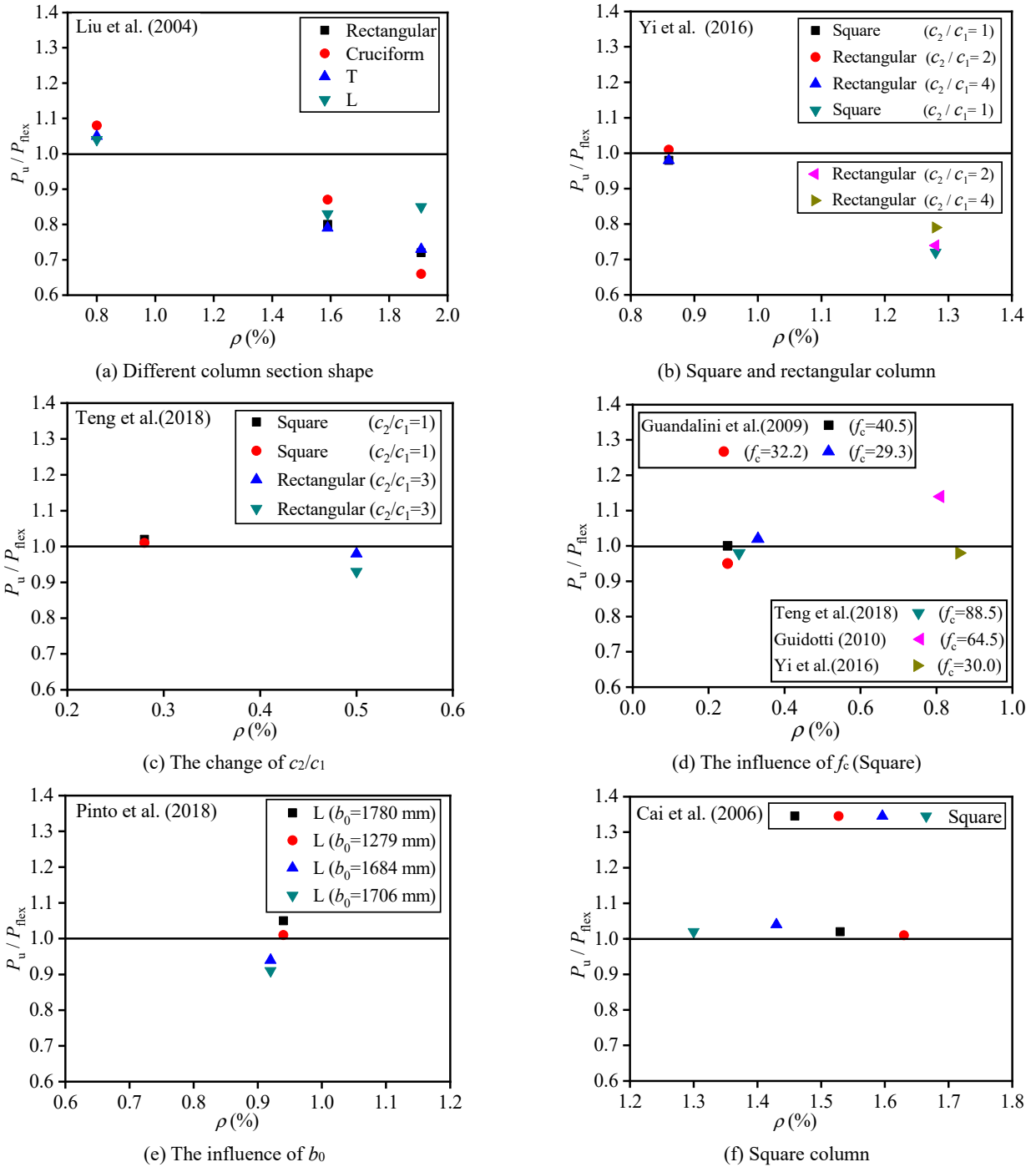


Fig. 8 Evaluation results

The reinforcement ratio between 0.9% and 1.3% belongs to bending-punching failure. The failure mode is mainly punching failure, but it is accompanied by bending characteristics, see Fig. 8(e). Based on the above analysis and combined with the test results, in order to better study the bearing capacity of slab-column connections under bending failure, the follow-up only focuses on the case where the ratio of the test results to the theoretical calculation results is greater than 1.

Based on the above results and appendix 1, the following conclusions can be drawn: i) The bending capacity of slab-special-shaped column connections estimated

by the formula based on the yield-line theory is basically consistent with the test results, which provides an acceptable accuracy; ii) For the rectangular column, the change of column limb length to thickness ratio (c_2/c_1) and concrete strength (f_c) has less influence on the bending capacity of slab-column connections under the same reinforcement ratio (see Figs. 8(b), 8(c) and 8(d)); iii) For L-shaped columns, there is no significant change in bending capacity with the increase or decrease of control perimeter (b_0) of column section under the same reinforcement ratio (see Fig. 8(e)).

4.2 Influence of column section shape on bending capacity

This section mainly studies the influence of column section shape on bending capacity. In order to study the influence of column section shape on bending capacity and ensure the singleness of analysis variables, the following assumptions are made before the analysis.

Assuming that the special-shaped column has the same section perimeter (l) and m_u , at the same time, ignoring the influence of internal displacement of slab support and size effect, $L_0 = L = l$. For the special-column, $c_1 + c_2 = l/2$ can be obtained; For the rectangular column, $4c_2 = l$ can be obtained; In addition, it is assumed that $\omega = c_2/c_1$. It is worth noting that as a correlation indicator, ω close to 1 indicates that the column section tends to be regular.

(1) Rectangular column

$$P_{\text{flex}} = \frac{4m_u[l + (2L(\omega + 1) - l\omega) \tan \alpha]}{2L(\omega + 1) - l\omega} + 4m_u[2L(\omega + 1) - l - \frac{(2L(\omega + 1) - l\omega) \tan \alpha}{[2L(\omega + 1) - l\omega](1 + \tan \alpha)}] + 4m_u[2L(\omega + 1) - l\omega - \frac{(2L(\omega + 1) - l) \tan \gamma}{[2L(\omega + 1) - l](1 + \tan \alpha)}] + \frac{4m_u[l\omega + (2L(\omega + 1) - l) \tan \gamma]}{2L(\omega + 1) - l} \quad (46)$$

(2) Cruciform column

$$P_{\text{flex}} = \frac{8m_u}{4L - l} \left[\frac{l}{\omega} + (4L - l) \tan \alpha + \frac{4\omega L - l - \omega(4L - l) \tan \alpha}{\omega(1 + \tan \alpha)} \right] \quad (47)$$

(3) T-shaped column

$$P_{\text{flex}} = 8m_u(\sqrt{2} - 1) + \frac{2m_u l(\omega + 3)}{(4L - l)\omega} + 2m_u(\tan \theta + \tan \eta) + \frac{4m_u}{(4L - l)(1 + \tan \theta)} \left[\frac{\omega(4L + l) - 2l - \omega(4L - l) \tan \theta}{\omega} \right] + \frac{2m_u}{(4L - l)(1 + \tan \theta)} \left[\frac{(4\omega L - l) - \omega(4L - l) \tan \theta}{\omega} \right] \quad (48)$$

(4) L-shaped column

$$P_{\text{flex}} = 2m_u[6(\sqrt{2} - 1) + \tan \eta] + \frac{4m_u(l + \omega l)}{\omega(4L - l)} + \frac{2m_u}{(4L - l)} \times \left[\frac{\omega(4L + l) - 2l - \omega(4L - l) \tan \eta}{\omega(1 + \tan \eta)} \right] \quad (49)$$

The parameters of each specimen were brought into Eqs. (46)-(49) and their bending capacity is calculated respectively. The results are shown in Fig. 9.

Fig. 9 shows the influence of column section shape on the bending capacity. It can be observed from Fig. 9 that the bending capacity of special-shaped columns with equal column section perimeter has the following relationship: T-shaped column > rectangular column > L-shaped column > cruciform column. In addition, the bending capacity does not change much with the column limb length to thickness ratio (c_2/c_1). Specifically, it can be concluded as follows: i) for the column section of equal perimeter, the bending capacity of T-shaped column is slightly higher than that of other three sections, but the magnitude of the increase is small. Obviously, the influence of the column section shape on the bending capacity is relatively limited; ii) the influence of the change of c_2/c_1 on the bending capacity of the connection does not exceed 6%, indicating that the

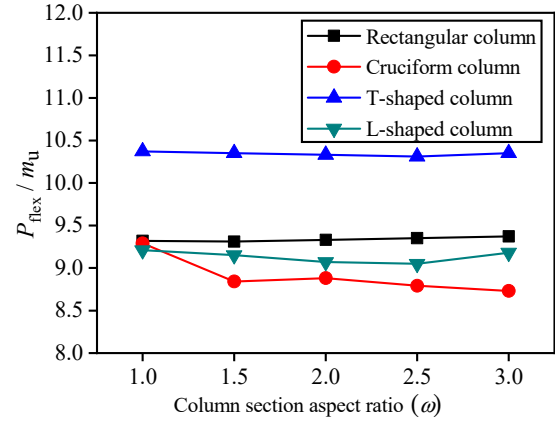


Fig. 9 P_{flex}/m_u - ω curves for different column section shape

influence of column section shape on the bending capacity can be ignored.

To further demonstrate this point, taking the rectangular column slab connection as an example, the calculation results and the test results in references (Al-Yousif and Regan 2003, Teng *et al.* 2004, Guandalini *et al.* 2009 and Yi *et al.* 2016) are compared and analyzed. A total of 16 rectangular column test results were collected, and the specific comparison results are shown in Fig. 10. It is not difficult to find that when the slab–rectangular column connection is subjected to concentrated load, the bending capacity of the connection decreases slightly with the increase of the column section from 1 to 4, but the overall state is flat. Therefore, for the slab–rectangular column connection, it can be concluded that the change of c_2/c_1 has little influence on the bending capacity of the slab–column connection. However, since there are few test results on the influence of large change of c_2/c_1 on the flexural capacity, it

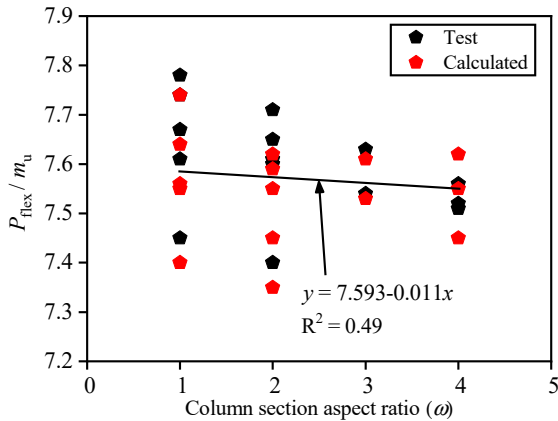


Fig. 10 P_{flex}/m_u - ω curves for rectangular column

is difficult to carry out further analysis.

5. Conclusions

In this paper, using the yield-line theory, a new set of general expressions for calculating the bending capacity of slab-special-shaped connections are proposed, and the following conclusions can be obtained.

- (1) Based on the yield-line theory, a formula for calculating the bending capacity of the slab-special-shaped column is established, and compared with the test results. The results shown that the theoretical solution derived in this paper has the characteristics of small dispersion rate and high accuracy, which can be used as reference for corresponding engineering applications.
- (2) After verifying the theoretical solution of bending capacity based on yield-line theory, the sensitivity of column section shape to the bending capacity of slab-special-shaped column connections was studied. The results show that the column section shape has an influence on the bending capacity of slab-column connection, but the influence is not obvious. At the same time, the influence of the column limb length to thickness ratio (c_2/c_1) on the bending capacity of special-shaped columns can be ignored.
- (3) For the rectangular column section, when the change of column limb length to thickness ratio (c_2/c_1) increases from 1 to 4, the bending capacity of the connection has no obvious change. However, the influence of the greater c_2/c_1 variation on bending capacity needs to be further explored.

Acknowledgments

This work is supported by National Natural Science Foundation of China (Grant No. 51708289).

References

- ACI Committee 318 (2011), Building Code requirements for structural concrete and commentary, American Concrete Institute.
- Al-Yousif, A.T. and Regan, P.E. (2003), "Punching resistance of RC slabs supported by large and/or elongated columns", *Struct. Eng.*, **81**(5), 30-34.
- Alam, A., Amanat, K.M. and Seraj, S.M. (2016), "An experimental study on punching shear behavior of concrete slabs", *Adv. Struct. Eng.*, **12**(2), 257-265. <https://doi.org/10.1260/136943309788251650>
- Baskaran, K. and Morley, C.T. (2004), "Using yield line theory for interior panels of slabs", *Proceedings of the Institution of Civil Engineers-Structures and Buildings*, **157**(6), 395-404. <https://doi.org/10.1680/stbu.2004.157.6.395>
- Bhowmik, T., Tan, K.H. and Balendra, T. (2017), "Lateral load-displacement response of low strength CFRP-confined capsule-shaped columns", *Eng. Struct.*, **150**, 64-75. <http://dx.doi.org/10.1016/j.engstruct.2017.07.037>
- Braestrup, M.W. (2008), "Yield line theory and concrete plasticity", *Mag. Concrete Res.*, **60**(8), 549-553. <https://doi.org/10.1680/mac.2008.60.8.549>
- Burgess, I. (2017), "Yield-line plasticity and tensile membrane action in lightly-reinforced rectangular concrete slabs", *Eng. Struct.*, **138**, 195-214. <https://doi.org/10.1016/j.engstruct.2017.01.072>
- Cai, J., Li, G., Yang, C. and Lin, F. (2006), "Tests on unbonded post tensioned concrete flat slab with T-shaped column connections", *Adv. Struct. Eng.*, **9**(5), 671-685. <https://doi.org/10.1260/136943306778827501>
- Chanthabouala, K. and Teng, S. (2015), "Failures of slabs having low bending steel ratios subjected to punching loads", *Proceedings of the 2015 World Congress on Advances in Structural Engineering and Mechanics*, Incheon, Korea, August.
- Cho, S.K., Kwark, J.W., Lee, J.M. and Moon, D.J. (2006), "Punching shear behavior of high-strength lightweight concrete slab under concentrated load", *KSCCE J. Civil Environ. Eng. Res.*, **26**(1A), 219-228.
- Elsheikh, M.A. (2006), "Analysis of R.C. slabs by Yield Line Theory", Department of Civil Engineering, Dspace University of Khartoum, Khartoum, Sudan.
- Eurocode 2 (1992), Design of Concrete Structures-Part 1: General rules and rules for building, Committee European de Normalization.
- GB 50010-2010 (2010), Code for design of concrete structure, Architecture & Building Press, Beijing, China.
- Ghali, A., Gayed, R.B. and Dilger, W. (2015), "Design of Concrete Slabs for Punching Shear: Controversial Concepts", *ACI Struct. J.*, **112**(4), 505-514.
- Goswami, A., Adhikary, S.D. and Li, B. (2019), "Predicting the punching shear failure of concrete slabs under low velocity impact loading", *Eng. Struct.*, **184**(8), 37-51. <https://doi.org/10.1016/j.engstruct.2019.01.081>
- Guandalini, S., Burdet, O. and Muttoni, A. (2009), "Punching tests of slabs with low reinforcement ratios", *ACI Struct. J.*, **106**(10), 87-95. <https://doi.org/10.14359/56287>
- Guidotti, R. (2010), "Poinçonnement des planchers-dalles avec colonnes superposées fortement sollicitées", Ph.D. Dissertation; École Polytechnique Fédérale de Lausann, Lausanne, Switzerland.
- Inácio, M.M.G., Lapi, M. and Ramos, A.P. (2020), "Punching of reinforced concrete flat slabs – Rational use of high strength concrete", *Eng. Struct.*, **206**, 110194. <https://doi.org/10.1016/j.engstruct.2020.110194>
- Kennedy, G. and Goodchild, C.H. (2004), *Practical Yield Line Design*, Concrete Centre, Surrey, UK.

- Liu, L. (2006), “Test study on punching shear strength of RC slabs with the effect of column aspect ratios and bending reinforcement ratios”, Ph.D. Dissertation; China Academy of Building Research, Beijing, China.
- Liu, W. and Huang, C. (2004), “Test investigation on punching shear behavior of concrete slab-nonrectangular column connections”, *J. Build. Struct.*, **25**(4), 26-33. <https://doi.org/10.14006/j.jzjgxb.2004.04.005>
- Liu, Sh. and Zhang, T. (2008), *Fundamental Theory of Elastic-Plastic Mechanics*, Huazhong University of Science and Technology Press, Wuhan, China.
- Ma, Y.C. and Lü, X.L. (2001), “Seismic behavior of reinforced concrete slab-column system”, *J. Build. Struct.*, **22**(4), 49-54. <https://doi.org/10.3321/j.issn:1000-6869.2001.04.009>
- Ma, H., Xi, J., Zhao, Y. and Dong, J. (2021), “Mechanical behaviour of composite columns composed of rac-filled square steel tube and profile steel under eccentric compression loads”, *Steel Compos. Struct., Int. J.*, **38**(1), 103-120. <https://doi.org/10.12989/scs.2021.38.1.103>
- Mamede, N., Ramos, A. and Faria, D. (2013), “Experimental and parametric 3D nonlinear finite element analysis on punching of flat slabs with orthogonal reinforcement”, *Eng. Struct.*, **48**, 442-57. <https://doi.org/10.1016/j.engstruct.2012.09.035>
- Osman, M., Marozuk, H. and Helmy, S. (2000), “Behavior of high-strength lightweight concrete slabs under punching loads”, *ACI Struct. J.*, **97**(3), 492-498.
- Park, R. and Gambe, W.L. (1980), *Reinforced concrete slabs*, New York, USA.
- Pinto, V.C., Branco, V. and Oliveira, D.R. (2018), “Punching in two-way RC flat slabs with openings and L section columns”, *Eng. Computat.*, **36**(7), 2430-2444. <https://doi.org/10.1108/EC-12-2018-0596>
- Quintas, V. (2003), “Two Main Methods for Yield Line Analysis of Slabs”, *J. Eng. Mech.*, **129**(2), 223-231. [https://doi.org/10.1061/\(ASCE\)0733-9399\(2003\)129:2\(223\)](https://doi.org/10.1061/(ASCE)0733-9399(2003)129:2(223))
- Sagaseta, J., Tassinari, L. and Ruiz, M.F. (2014), “Punching of flat slabs supported on rectangular columns”, *Eng. Struct.*, **77**(77), 17-33. <https://doi.org/10.1016/j.engstruct.2014.07.007>
- Shubha, D.K., Lavina, E.J. and Indrani, V. (2014), “Dynamic analysis of multistory rcc building frame with flat slab and grid slab”, *J. Eng. Res. Appl.*, **4**(2), 416-420.
- Stein, T., Ghali, A. and Dilger, W. (2007), “Distinction between punching and flexural failure modes of flat plates”, *ACI Materials J.*, **104**(3), 357-365.
- Teng, S., Cheong, H.K. and Kuang, K.L. (2004), “Punching shear strength of slabs with openings and supported on rectangular columns”, *ACI Struct. J.*, **101**(5), 678-687.
- Teng, S., Chanthabouala, K., Lim, D.T. and Hidayat, R. (2018), “Punching shear strength of slabs and influence of low reinforcement ratio”, *ACI Struct. J.*, **115**(1), 139-150. <https://doi.org/10.14359/51701089>
- Thomas, W.H. (2004), “Bending-punching shear interaction in an oriented strand board”, *J. Mater. Civ. Eng.*, **16**(4), 341-348. [https://doi.org/10.1061/\(ASCE\)0899-1561\(2004\)16:4\(341\)](https://doi.org/10.1061/(ASCE)0899-1561(2004)16:4(341))
- Tovi, S., Goodchild, C. and Jahromi, A.B. (2017), “Deformation of multi-storey flat slabs, a site investigation”, *Adv. Concrete Constr.*, **5**(1), 49-63. <http://dx.doi.org/10.12989/acc.2017.5.1.049>
- Yi, W., Zou, P. and Deng, Q. (2016), “Test study of the effects of cross-sectional shape of column on punching shear performance of slab-column connection”, *China Civil Eng. J.*, **49**(5), 87-95. <https://doi.org/10.15951/j.tmgcxb.2016.05.008>
- Zhou, L., Huang, Y. and Chen, B. (2021), “Punching shear behavior of slab–column connections embedded with steel skeletons”, *Struct.*, **33**(1-3), 2879-2892. <https://doi.org/10.1016/j.istruc.2021.06.052>
- Zhu, B., Tu, Ch. and Yu, A. (1993), *Design Principles of Concrete*

Structures, Tongji University Press, Shanghai, China.

CC

Notation

f_y	yield strength of flexural reinforcement
f_c	concrete compressive strength
f_{cm}	design value of compressive strength of concrete
b_0	control perimeter
ω	column section aspect ratio
h_0	effective thickness of the slab
A_s	area of tensile reinforcement per unit width
ρ	reinforcement ratio of tensile reinforcement
δ	node displacement
W_e	external work
W_i	virtual work
m	bending moment
m_u	ultimate bending moment per unit length
m_x	ultimate bending moment per unit length in x direction
m_y	ultimate bending moment per unit length in y direction
c	side length of square column
c_1	column section limb thickness
c_2	column section limb length
L	side length of the slab
L_0	effective side length of slab
l_0	yield-line of length
l	perimeter of special-shaped column section
θ_n	relative angle of rotation between yield-lines
$\alpha, \beta, \lambda, \theta, \eta, \varphi, \gamma$	direction angle between the yield-line
P	concentrated load
P_i	unit concentrated load
P_{flex}	calculated bending bearing capacity
P_u	ultimate bearing capacity test result

Appendix A1

Test data

Source	Serial No.	Section shape	L/mm	h/mm	c_2/mm	c_1/mm	f_c/Mpa	f_y/Mpa	$\rho/\%$	P_u/kN	P_{flex}/kN
Liu and Huang (2004)	CS-1	cruciform	1500	140	300	100	36.4	377.0	1.59	533	613
	CT-1	T	1500	140	300	100	42.3	377.0	1.59	584	735
	CL-1	L	1500	140	300	100	34.2	377.0	1.59	520	628
	CF-1	square	1500	140	300	300	38.3	377.0	1.59	520	652
	CS-2	cruciform	1500	140	300	100	30.1	377.0	1.91	473	712
	CT-2	T	1500	140	300	100	38.4	377.0	1.91	633	862
	CL-2	L	1500	140	300	100	40.9	377.0	1.91	637	753
	CF-2	square	1500	140	300	300	39.6	377.0	1.91	557	772
	CS-3	cruciform	1500	140	300	100	37.4	377.0	0.80	440	408
	CT-3	T	1500	140	300	100	38.9	377.0	0.80	408	388
CL-3	L	1500	140	300	100	41.9	377.0	0.80	405	389	
Cai <i>et al.</i> (2006)	P150-1	T	2200	150	720	180	38.7	280.1	1.53	600	588
	P150-2	T	2200	150	720	180	37.7	280.1	1.63	640	652
	P150-3	T	2200	150	720	180	40.5	280.1	1.43	560	538
	P180-1	T	2200	180	720	180	38.7	280.1	1.30	900	881
Guandalini <i>et al.</i> (2009)	PG-2b	square	3300	250	260	260	40.5	552.0	0.25	440	441
	PG-4	square	3300	250	260	260	32.3	541.0	0.25	408	430
	PG-5	square	3300	250	260	260	29.3	555.0	0.33	550	537
	PG-10	square	3300	250	260	260	28.5	577.0	0.33	540	557
Guidotti (2010)	PT22	square	3000	220	260	260	64.5	552	0.82	839	857
	PG20	square	3000	220	260	260	50.6	551	1.56	860	887
Yi <i>et al.</i> (2016)	CL-1	square	2550	180	250	250	30.0	453.6	0.86	507	518
	CL-2	rectangular	2550	180	330	170	28.2	453.6	0.86	516	512
	CL-4	rectangular	2550	180	400	100	28.6	453.6	0.86	498	511
Teng <i>et al.</i> (2018)	S11-28	square	2200	150	200	200	88.5	459.6	0.28	280	274
	S11-50	square	2200	150	200	200	88.5	537.2	0.50	394	404
	S13-28	rectangular	2200	150	600	200	90.1	459.4	0.28	308	306
	S13-50	rectangular	2200	150	600	200	90.1	537.5	0.50	418	449
Pinto <i>et al.</i> (2018)	L-R	L	1800	120	400	100	25.0	538.0	0.94	285	271
	L-1	L	1800	120	400	100	25.0	538.0	0.94	273	269
	L-2	L	1800	120	400	100	25.0	538.0	0.92	275	294
	L-3	L	1800	120	400	100	25.0	538.0	0.92	277	303